# Journal of Materials Chemistry C

Accepted Manuscript


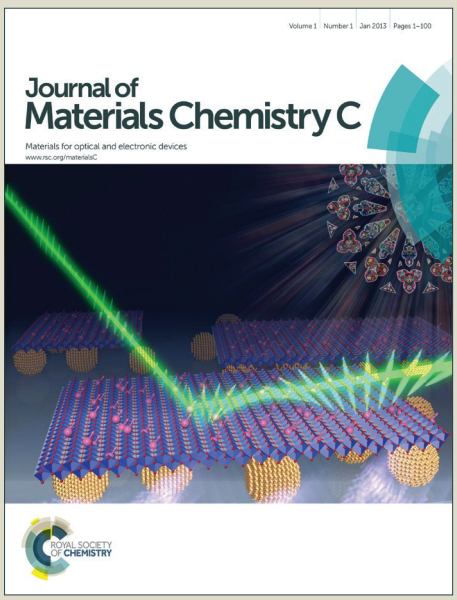





ROYAL SOCIETY OF CHEMISTRY

www.rsc.org/materialsC

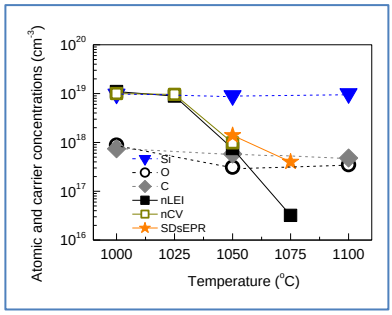


While increasing temperature is essential for reducing carbon and oxygen incorporation, it reduces the incorporation of silicon as a donor.

Journal Name

ARTICLE

# *n*-type conductivity bound by the growth temperature: the case of $Al_{0.72}Ga_{0.28}N$ highly doped by silicon

Received 00th January 20xx,
Accepted 00th January 20xx

DOI: 10.1039/x0xx00000x

www.rsc.org/

A. Kakanakova-Georgieva,[a] S.-L. Sahonta,[b] D. Nilsson,[a] X. T. Trinh,[a] N. T. Son, [a] E. Janzén,[a] and C. J. Humphreys[b]

High-Al-content $Al_xGa_{1-x}N$ layers, x ~ 0.72, have been grown by metal organic chemical vapour deposition (MOCVD) at a temperature ranging from 1000 to 1100 °C, together with high flow rate of the dopant precursor silane ($SiH_4$) in order to obtain highly Si-doped $Al_{0.72}Ga_{0.28}N$ layers, ~ $1 \times 10^{19}$ $cm^{-3}$ as measured by secondary ion mass spectrometry (SIMS). Further characterization of the layers by capacitance-voltage (C-V), electron paramagnetic resonance (EPR), and transmission electron microscopy (TEM) measurements reveals the complex role of growth temperature for the *n*-type conductivity of high-Al-content $Al_xGa_{1-x}N$. While increasing temperature is essential for reducing the incorporation of carbon and oxygen impurities in the layers, it also reduces the amount of silicon incorporated as a donor.

## Introduction

Establishing *n*- and *p*-type conductivity in epitaxial layers *via* intentional doping is fundamental to any semiconductor material system and its relevant device applications. Growth parameters such as temperature, gas-flow-rate of precursors and pressure may all affect intentional doping in epitaxial layers grown by metal organic chemical vapour deposition (MOCVD). The same growth parameters, particularly temperature, also affect the incorporation of carbon and oxygen impurities which has been observed in the MOCVD of III-V semiconductor materials such as $Al_xGa_{1-x}As$ and GaN.

In the case of GaN, an original study has reported that an increase in growth temperature from around 955 to 1065 °C reduces the incorporation of carbon, which mainly originates from the hydrocarbon fragments of the metal organic precursor trimethylgallium, $(CH_3)_3Ga$, by a factor of up to 25 [1]. The understanding is that the increased growth temperature leads to enhanced generation of hydrogen radicals from the principal precursor ammonia, $NH_3$, and the carrier gas hydrogen, $H_2$, which combine with hydrocarbon fragments on the layer surface to give methane, $CH_4$, which then desorbs from the surface [1]. Carbon acts as an acceptor in GaN and $Al_xGa_{1-x}As$ materials by substituting N and As atoms, respectively, in the crystal lattice. The strong dependence of the carbon concentration on the temperature has been utilized in the epitaxial growth of various device structures such as (i) multi-junction solar cells, which include $p^{++}$-$Al_xGa_{1-x}As$ layers doped by carbon at the optimal growth temperature for this material system, typically ranging from 510 to 630 °C [2], and (ii) GaN-based high-electron-mobility transistors, which include semi-insulating GaN buffer layers with optimized concentration of the carbon impurities [3] which can also be achieved by varying the growth temperature from 980 to 1080 °C [4].

An increase in growth temperature reduces the incorporation of oxygen impurities in semiconductor alloys containing Al, such as $Al_xGa_{1-x}As$ [5], and $Al_xGa_{1-x}N$ [6-8]. The incorporation of oxygen into $Al_xGa_{1-x}N$ alloys, where oxygen substitutes for N in the crystal lattice ($O_N$), has an instant impact on the conductivity of respective layers. From experiment and various density functional theory (DFT) calculations, it has been found that $O_N$ is an effective-mass donor in GaN with a fourfold-coordinated geometry [9, 10]. The incorporation of oxygen into AlN gives rise to strongly localized states associated with the so-called DX centers in the material, which have been described to involve a "large, bond-rupturing displacement" of the donor atom itself, or one of its nearest-neighbour atoms, along a bond axis [11]. The large extent of lattice relaxation is accompanied by the trapping of an extra electron, therefore reducing the carrier concentration in the conduction band and limiting the conductivity. DFT calculations attest to the formation of oxygen-related DX centers in AlN independent of the functional used [9, 10]. The most recent DFT calculations using the screened hybrid functional of Heyd, Scuseria, and Ernzerhof (HSE) predict that the onset for oxygen-related DX center formation in $Al_xGa_{1-x}N$ alloys occurs for x > 0.61 with an uncertainty in the order of 0.1 [12].

DX centers have been identified by the presence of persistent photoconductivity at low temperatures in a number

[a] Department of Physics, Chemistry and Biology (IFM), Linköping University, SE 581 83 Linköping, Sweden
[b] Department of Materials Science and Metallurgy, University of Cambridge, 27 Charles Babbage Road, Cambridge, CB3 0FS, UK.

of semiconductors, including $Al_xGa_{1-x}As$ where $0.22 < x < 0.8$, doped by Te [13], $Al_{0.39}Ga_{0.61}N$ doped by oxygen [14], and AlN doped by Si [15]. The formation of DX centers in semiconductor materials, for example silicon-doped $Al_xGa_{1-x}As$ [16], $Al_xGa_{1-x}N$ [17] and AlN [15, 18], have been explored by the application of electron paramagnetic resonance (EPR) measurements, which extract data about the interaction between the electron spin and nuclear spin of the impurity (defect) and to the neighbouring atoms, and can provide unique information as to the chemical nature of the defect and defect concentration.

It is clear from the above introduction that an increase in growth temperature would benefit the *n*-type conductivity of high-Al-content $Al_xGa_{1-x}N$ layers where $x > 0.60 \sim 0.70$. An increase in growth temperature reduces the incorporation of carbon and oxygen impurities, and consequently inhibits the formation of related compensating defects. In the present study we select *n*-type $Al_{0.72}Ga_{0.28}N$ layers which have been highly doped by silicon to the atomic concentration of [Si] ~ $1 \times 10^{19}$ $cm^{-3}$. Most importantly, the $Al_{0.72}Ga_{0.28}N$:Si layers, when grown at 1000 °C, exhibit a low electrical resistivity of $\rho \sim 0.012$ Ω·cm, which compares well with reference values [19-21]. *n*-type $Al_{0.70}Ga_{0.30}N$:Si layers can exhibit a minimum electrical resistivity of $\rho \sim 0.0075$ Ω·cm when doped by silicon to a higher concentration of [Si] ~ $3.5 \times 10^{19}$ $cm^{-3}$ [19]. We note that the electrical resistivity of high-Al-content $Al_xGa_{1-x}N$ layers depends strongly on the Al content. The electrical resistivity is known to increase by up to four orders of magnitude for AlN layers compared to layers of $Al_{0.70}Ga_{0.30}N$ alloy, which correlates with a respective decrease in the carrier concentration [19-21]. It has been reported that $Al_{0.96}Ga_{0.04}N$:Si layers with optimized structural quality and doping characteristics exhibit electrical resistivity of $\rho \sim 3.35$ Ω·cm, yet enabling efficient light emitting diodes in the deep ultraviolet spectral range [21].

Using the low resistivity of the *n*-type $Al_{0.72}Ga_{0.28}N$:Si layers grown at 1000 °C as a reference point, we targeted further improvement of the transport properties of the layers by an increase in growth temperature. We will show that an increase in growth temperature can indeed achieve layers with reduced incorporation of oxygen and carbon impurities. However, implementation of high growth temperatures in combination with high flow rates of the dopant precursor silane ($SiH_4$) in order to obtain highly Si-doped $Al_{0.72}Ga_{0.28}N$ layers can potentially limit doping efficiency and conductivity.

## Experimental

In this study, $Al_{0.72}Ga_{0.28}N$:Si/$Al_{0.72}Ga_{0.28}N$/AlN structures were grown on semi-insulating 4H-SiC substrates in a horizontal hot-wall MOCVD reactor (GR508GFR AIXTRON). The SiC substrates were heated up in the flow of hydrogen gas. The reactor was operated at a process pressure of 50 mbar. Trimethylaluminum, TMAl, of semiconductor grade, trimethylgallium, TMGa, of semiconductor grade, ammonia, $NH_3$, (99.9999%); and silane, $SiH_4$, (99.999%) diluted to 200 ppm in $H_2$ (99.9996%) were used as precursors. The effective substrate template, AlN-on-SiC, was overgrown by a composition-graded $Al_xGa_{1-x}N$ layer with *x* decreasing from 1.0 to 0.72 by lowering the growth temperature from 1240 °C (the temperature for the AlN growth) to any of the set values of 1000, 1025, 1050, 1075, and 1100 °C (the various temperatures for the $Al_{0.72}Ga_{0.28}N$ growth in this study). TMGa was introduced at a constant gas-flow-rate corresponding to the alloy composition of $x \sim 0.72$ during the deposition of the graded layer. A high gas-flow-rate ratio of $SiH_4$/(TMAl+TMGa) of ~ $1.0 \times 10^{-3}$ was applied. The layers of $Al_{0.72}Ga_{0.28}N$ (including doping) were deposited at a growth rate of ~ 460 nm/h. The concentration of dopants and residual impurities, and the alloy composition were measured by secondary ion mass spectrometry (SIMS). The SIMS measurements were obtained through a commercial analytical service [22]. With Cs primary ion bombardment, Al, and Ga measurements were obtained using positive secondary ion detection. Si, C, and O depth profiles were obtained in another measurement by acquiring negative secondary ions. The quantification of the Al content and Si, C, and O concentrations was performed using proprietary data processing method PCOR-SIMS [22]. The instrument conditions were optimized for overall depth resolution and sensitivity. The mobility and carrier concentration were measured by a microwave-based contactless mobility measurement system (LEI 1610, Lehighton Electronics, Inc.). Capacitance-voltage (C-V) measurements were performed on Schottky contacts formed on the $Al_xGa_{1-x}N$:Si layers using a mercury probe at 1 kHz (HP4284A LCR meter and PRC100 mercury probe station). EPR measurements were performed on an X-band (~9.4 GHz) Bruker E500 EPR spectrometer equipped with a continuous He flow cryostat, allowing control of the sample temperature from 4 to 295 K. Specimens were prepared in cross-section for transmission electron microscopy (TEM) by mechanical polishing and ion milling using $Ar^+$ ions accelerated to 5 kV until a perforation was observed in the SiC substrate. Specimens were studied using a Philips CM30 TEM operating at 300 kV and a JEOL 4000EX TEM operating at 400 kV.

## Results and discussion

As already pointed out, the $Al_{0.72}Ga_{0.28}N$:Si layers grown at 1000 °C exhibit a low electrical resistivity of $\rho \sim 0.012$ Ω·cm. The low electrical resistivity results from the high doping of [Si] ~ $1 \times 10^{19}$ $cm^{-3}$, which gives rise to a carrier concentration of $n \sim 1 \times 10^{19}$ $cm^{-3}$. The carrier concentration was obtained using C-V measurements and microwave-based contactless measurements (labelled nCV, and nLEI, respectively, on the plot in Figure 1).

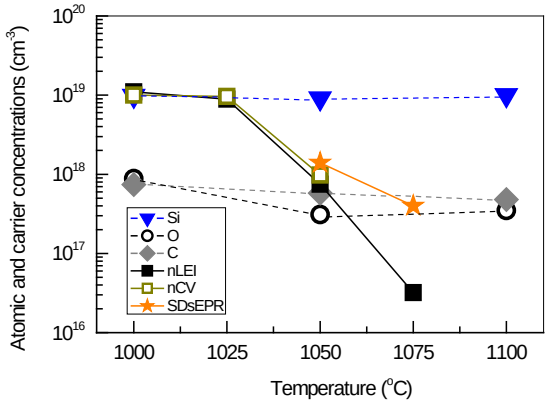


**Fig. 1** Temperature dependence of the atomic concentration of silicon, oxygen, and carbon; the carrier concentration (n) obtained by C-V (nCV) and contactless microwave-based (nLEI) measurements; and the concentration of silicon donor on the neutral charge state (SDs) estimated by EPR.

The high correlation between the silicon concentration and carrier concentration in the $Al_{0.72}Ga_{0.28}N$:Si layers grown at 1000 °C indicates no major effect of carrier compensation. $Al_{0.72}Ga_{0.28}N$:Si layers were further grown at each of the higher temperatures of 1025, 1050, 1075, and 1100 °C. At each of these temperatures, silicon was incorporated into the layers at the same concentration of [Si] ~ $1 \times 10^{19}$ cm$^{-3}$ as verified by SIMS for the layers grown at 1050 and 1100 °C (Fig. 1). The concentrations of both the oxygen and carbon impurities are at least an order of magnitude lower than that of silicon for any of the growth temperatures. Particularly, the oxygen concentration decreases by a factor of three with an increase in temperature from 1000 to 1100 °C, as in Fig. 1. In the layer grown at the highest temperature of 1100 °C, the concentrations of oxygen and carbon impurities correspond to the values at the typical SIMS instrument detection limit for silicon and oxygen in AlN, respectively, [O] ~ $2 \times 10^{17}$ cm$^{-3}$ and [C] ~ $2 \times 10^{17}$ cm$^{-3}$. The highest growth temperature of 1100 °C causes an increase in the Al content in the layer and is understood to be due to the lower thermal stability of GaN than AlN. According to the SIMS measurements, this results in the growth of an $Al_{0.77}Ga_{0.23}N$:Si (instead of $Al_{0.72}Ga_{0.28}N$:Si) layer at 1100 °C. The growth of higher-Al-content alloy at 1100 °C has been confirmed by EPR measurements of the structures grown at 1100 °C, 1075 °C, and 1050 °C, respectively, whereby the associated g-values are consistent with the corresponding EPR spectra [8]. The higher-Al-content layer grown at 1100 °C is then excluded from further considerations in this study.

Both, C-V measurements and microwave-based contactless measurements, indicate a constant value of $n \sim 1 \times 10^{19}$ cm$^{-3}$ for the layers with the lowest two temperatures of 1000 and 1025 °C, but $n$ decreases for layers grown at the higher temperatures of 1050 and 1075 °C (Fig. 1). It is clear from the SIMS studies that the low carrier concentration has no correlation with the oxygen, carbon, and Al contents in the layers, but most probably with the amount of silicon incorporated as a donor. The concentration of incorporated silicon donors was estimated based on EPR measurements.

The EPR measurements were performed on the $Al_{0.72}Ga_{0.28}N$:Si structures grown at 1050 and 1075 °C; the $Al_{0.72}Ga_{0.28}N$:Si structures grown at 1000 and 1025 °C have too high a conductivity and could not be measured by EPR due to microwave coupling problems. The EPR signal [8] could be detected in darkness at a sample temperature of T = 5 K and up to T = 250 K. Respective EPR signals detected in darkness at T = 100 K are plotted in Figure 2. The intensity of each EPR signal increases with temperature and exhibits a maximum in the temperature range of 70 to 120 K, beyond which the intensity drops. Such a temperature-dependent EPR signal is indicating for a DX center [17, 18].

It is necessary to provide the remark here that besides oxygen, the incorporation of silicon into AlN gives rise to DX centers. For the past decades, various DFT calculations using different functionals have generated controversy as to the formation of silicon-related DX centers in AlN. Recently, the HSE screened hybrid functional has been argued for a more accurate description of the DX centers that may form in AlN [10, 12]. Such recent calculations attest to the formation of stable and metastable Si-related DX centers in AlN [10]. EPR has previously been reported on Si-doped AlN layers grown on sapphire substrates by plasma induced molecular beam epitaxy [15], and more recently on unintentionally Si-doped bulk crystals of AlN grown by physical vapor transport [18], which observe the formation of silicon-related DX centers in AlN. The onset of silicon-related DX center formation in $Al_xGa_{1-x}N$ alloys requires investigation. Reports on EPR of high-Al-content $Al_xGa_{1-x}N$ are scarce and they include our most recently published data on $Al_xGa_{1-x}N$ layers of $0.79 \le x \le 1.0$ [17].

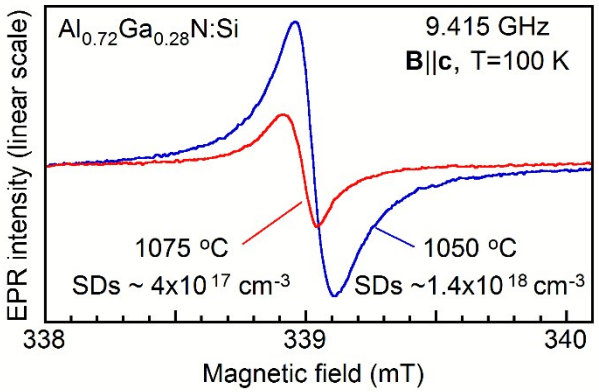


**Fig. 2** EPR signals of the shallow donor measured in darkness at 100 K for the magnetic field parallel to the c-axis (**B||c**) in $Al_{0.72}Ga_{0.28}N$:Si layers grown at 1050 and 1075 °C. The donor concentration on the neutral charge state estimated by EPR for each layer is indicated.

Accordingly [15], the understanding is that the conductivity in these layers is caused by the thermal emission of electrons from the associated stable Si-related $DX^-$ state into the conduction band, and the activation energy of the conductivity in these layers is related to the energy level of the associated stable Si-related $DX^-$ state [23], which was derived from the EPR measurements [17]. The negatively charged $DX^-$ state (occupied by two electrons) is the lowest-energy ground state of the Si donor [15]. More details on the proposed configuration-coordinate diagram of the Si donor in AlN can be followed in Ref. 15. Our EPR studies have shown, that for up to x ~ 0.83 the Si-related DX centers do not affect significantly the conductivity of the respective layers as the energy separation between the negatively charged $DX^-$ state and the neutral charge state of the Si donor is less than ~ 9 meV [17].

The maximum intensity of the EPR signal was used to estimate the maximum electron spin density, which is representative of the concentration of Si donors incorporated into the $Al_{0.72}Ga_{0.28}N$ (labelled as SDs on the plot in Figure 1). For that, detailed analysis of the temperature dependence of the intensity of the EPR signal was performed as previously applied to high-Al-content $Al_xGa_{1-x}N$ of $0.79 \leq x \leq 1.0$ [17]. This estimation results in SDs ~ $1 \times 10^{18}$ $cm^{-3}$ and ~ $4 \times 10^{17}$ $cm^{-3}$ respectively for the $Al_{0.72}Ga_{0.28}N$:Si structures grown at 1050 and 1075 °C. The estimated concentration of Si donors and concentration of carriers scale reasonably, moreover the same trend is exhibited with an increase in temperature between 1050 and 1075 °C (Fig. 1). However, SDs represents only a very small fraction of the total silicon atoms incorporated into the layers as measured by SIMS, [Si] ~ $1 \times 10^{19}$ $cm^{-3}$. In particular, the ratio SDs/[Si] is found to be ~ $10^{-1}$ and ~ $10^{-2}$ respectively, which correlates with an increase in growth temperature from 1050 to 1075 °C.

An increase in growth temperature can affect the relative rates of specific surface interactions during the stage of $SiH_4$ supply. It is likely that submonolayers of Si-N bonds can form within the microstructure of the layers, including at sites of nitrogen dangling bonds such as threading dislocation cores [24] and (1-101) facets [25]. In the case of treatment of the $Al_xGa_{1-x}N$ surface with Si-bearing precursor such as tetraethylsilicon, the formation of a submonolayer of Si-N bonds with varying "fractional coverage" has been reported depending on the amount of Si applied and the temperature [24]. The submonolayer coverage by Si-N bonds (generally referred to as a $SiN_x$ layer [26]) has widely been considered when the growing surface of GaN is exposed to a flash of silane flow. Some earlier TEM studies have identified this submonolayer to be in a certain structural relationship with GaN causing threading dislocations to bend towards the c-plane [27]. Recently, experimental proof for the $SiN_x$ layer has been obtained using aberration-corrected high resolution transmission electron microscopy [26]. In combination with DFT calculations, the atomic structure of this layer was proposed to be 2D $SiGaN_3$. The cited reference reported on the growth of a $SiN_x$ layer at a sharp 3D-2D transition boundary in GaN, therefore allowing easy observation. We could expect that in our case direct evidence of submonolayer coverage of Si-N bonds within the microstructure of the highly Si-doped $Al_{0.72}Ga_{0.28}N$ layers would be extremely difficult to observe with TEM.

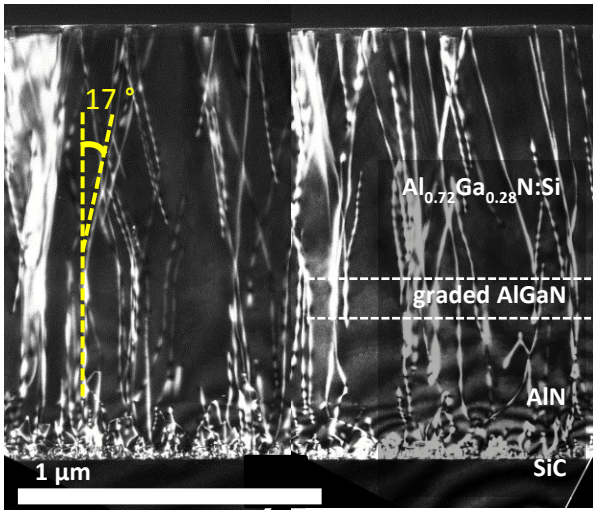


**Fig. 3** Dark field TEM image of a specimen taken with g = 1-100 close to the [11-20] zone axis. Threading a- and a+c-type dislocations are visible, propagating along the growth direction [0001].

Typical cross-sectional TEM images of the studied $Al_{0.72}Ga_{0.28}N$:Si/$Al_{0.72}Ga_{0.28}N$/AlN/SiC layer structures grown at the various temperatures show threading dislocations in $Al_{0.72}Ga_{0.28}N$ which propagate through the AlN layer after nucleation at the interface with the foreign SiC substrate, Fig. 3(a). Dislocation densities of around $1 \times 10^{10}$ $cm^{-2}$ were observed for all layers, with around 75 % of dislocations of pure edge type. The dislocation density appears to decrease dramatically after the deposition of around 150 nm AlN owing to the nucleation layer inducing the bending of threading dislocations into the c-plane, and those of opposite Burgers vector meet and annihilate [28]. Dislocations appear to incline to an angle of 17 ° with respect to [0001] in the upper $Al_{0.72}Ga_{0.28}N$ layer. The onset of this inclination is generally above the $Al_{0.72}Ga_{0.28}N$ interface with the composition-graded $Al_xGa_{1-x}N$ layer where x is decreasing from 1.0 to 0.72 by lowering the temperature from 1240 °C (the temperature for the AlN growth) to any of the set values of 1000, 1025, 1050, 1075 °C (the various temperatures for the $Al_{0.72}Ga_{0.28}N$ growth in this study). The composition-graded $Al_xGa_{1-x}N$ layer appears atomically-flat on the lower interface with the AlN, but appears rough at the upper interface, as shown in the scanning TEM image in Figure 4. This image was taken along the [11-20] zone axis using a high-angle annular dark-field (HAADF) electron detector which collects images in which atoms with high atomic number, such as gallium, appear with relative bright contrast and those with low atomic number, such as aluminium, appear with dark contrast. The upper region of the layer shows bright contrast due to the higher concentration of gallium atoms in the $Al_xGa_{1-x}N$ layer. The composition-graded $Al_xGa_{1-x}N$ layer shows a variation in contrast from dark to bright along [0001] as more

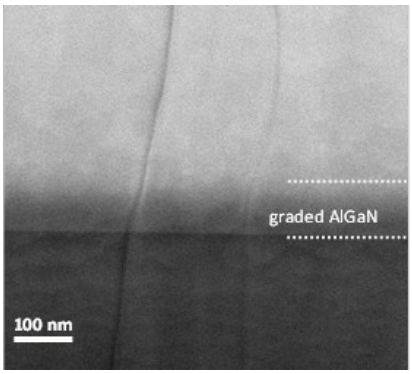


**Fig. 4** [11-20] HAADF TEM image of the graded AlGaN layer, showing two inclined dislocations.

gallium is incorporated into the layer. Two threading dislocations are visible which appear to increase their angle of inclination within the composition-graded $Al_xGa_{1-x}N$ layer, suggesting that some of the dislocations may begin to incline either within the composition-graded $Al_xGa_{1-x}N$ layer, as well as during the deposition of the subsequent $Al_{0.72}Ga_{0.28}N$ layer, and predominantly within the Si-doped $Al_{0.72}Ga_{0.28}N$ layer. The dislocations are viewed in projection in the cross-section specimens so the observed inclination angles range from zero to a maximum of around 17 ° according to the direction of travel of the dislocations through the TEM foil, as in Fig. 3(b).

The inclination of TDs in the $Al_xGa_{1-x}N$ material system is a recognized mechanism for compressive strain relaxation, followed by transition to a tensile strain, whereby thermodynamic calculations based on bulk-energy-balance provide a set of conditions for the onset of the inclination of TDs [29]. An alternative model can be provided when considering the kinetics of the growth of the composition-graded $Al_xGa_{1-x}N$ layer. The composition-graded $Al_xGa_{1-x}N$ was grown by the gradual reduction of the growth temperature, which resulted in an increase in the amount of gallium incorporated into the layer as growth proceeded. The ramp-down in temperature is also consistent with allowing kinetically-slower surface coverage processes to dominate, such as the incorporation of vacancies or the formation of localised surface pits at dislocation terminations during the deposition (in the case of the compressively-strained layers); however for layers under tension then the incorporation of self-interstitials or the formation of monolayer islands around dislocation cores would be required). This process is known as surface-mediated climb [30] and it can be further envisaged that any growth conditions that promote surface roughening are likely to enhance surface-mediated climb, as in the case of the graded layers in this study which exhibit rough upper surfaces. This is consistent with the work of Romanov et.al., [29] where silicon dopant was shown to increase the inclination angle of dislocations; the silicon is thought to act as an anti-surfactant and promote the surface-mediated climb process.

It can be inferred that the particular microstructure, which develops within the Si-doped $Al_{0.72}Ga_{0.28}N$ layer, and the speculated formation of coverage of Si-N bonds at the higher growth temperatures used in combination with a high $SiH_4$ flow rate, would prevent the incorporation of silicon atoms at substitutional donor sites such that they could contribute to doping. We can note that the detailed TEM study of the $Al_{0.72}Ga_{0.28}N$ layer structures presents the bending of the threading dislocations within the structures. It is known that inclination of threading dislocations represents a mechanism by which a tensile-stress-gradient is introduced in a typical $Al_xGa_{1-x}N$ layer structure along the growth direction, which can ultimately cause the build-in of a tensile strain [31, 32]. Following theoretical calculations, the incorporation of Si at substitutional acceptor site, $Si_N$, is considered energetically unfavorable unless the $Al_xGa_{1-x}N$ layer is under tensile stress, as the findings of a recent study may suggest [33]. This plausible effect contributes to the combination of effects that might be involved in explaining the lack of Si incorporation at substitutional donor sites as have been obtained by the EPR measurements in this study.

Formation of acceptor-type point defects such as group III vacancies ($V_{III}$) and complexes such as $V_{III}Si_{III}$ has also been invoked in explaining the mechanism of compensation in Si-doped high-Al-content $Al_xGa_{1-x}N$ layers where x~0.60 grown at various process conditions including temperature, V/III ratio, and doping concentration [6, 34]. The equilibrium concentration of group III vacancies in the crystal lattice of $Al_xGa_{1-x}N$ has been calculated to increase with increase in temperature [35], which was the argument in explaining the significant drop in carrier concentration, from ~ $2 \times 10^{18}$ $cm^{-3}$ to $1 \times 10^{17}$ $cm^{-3}$ with increase in temperature in a case study of $Al_{0.62}Ga_{0.38}N$ layer doped by silicon at ~ $3 \times 10^{19}$ $cm^{-3}$ [6]. A very recent report on the growth temperature dependence of Si doping efficiency in high-Al-content $Al_{0.70}Ga_{0.30}N$ also refers to thermodynamically driven compensating point defect formation in explaining the reduction of electron concentration (i.e. from $2.0 \times 10^{18}$ -> $1.1 \times 10^{18}$ -> $2.9 \times 10^{17}$ $cm^{-3}$) as the temperature has been increased from 1060 -> 1120 -> 1170 °C, respectively [36]. There is no data about the actual atomic concentration of the Si dopant incorporated into the $Al_{0.70}Ga_{0.30}N$ alloy. The reduction of the carrier concentration is reported to be accompanied with a reduction of the mobility (i.e., from 100 -> 71 -> 41 $cm^2V^{-1}s^{-1}$, respectively), and consequently explained as a further evidence for the excess point defect formation giving rise to heavy compensation effects [36]. We can note, that we observe an opposite trend in our present study. As the temperature increases from 1000 -> 1025 -> 1050 -> 1075 °C, and the electron concentration decreases from about $1.2 \times 10^{19}$ -> $8.9 \times 10^{18}$ -> $7.5 \times 10^{17}$ -> $3.3 \times 10^{16}$ $cm^{-3}$ for the same atomic concentration of the incorporated Si dopant, ~ $1 \times 10^{19}$ $cm^{-3}$, the mobility increases as 43 -> 50 -> 76 -> 270 $cm^2V^{-1}s^{-1}$. A major factor in the scattering mechanism in highly doped semiconductors is the scattering from ionized dopants. The trends in the measured values of the electron concentration and mobility thus confirm the findings of the EPR study that not all of the total silicon atoms incorporated into the layers, has contributed SDs.

## Conclusions

We have presented our understanding of the complex role of growth temperature for the *n*-type conductivity of high-Al-content $Al_xGa_{1-x}N$ highly doped by silicon, for the example of x ~ 0.72. We have shown that an increase in temperature can indeed achieve layers with reduced incorporation of oxygen and carbon impurities which otherwise could cause compensation through the formation of substitutional point defect $C_N$, and oxygen-related DX centers for certain values of x > 0.70. However, we find that implementation of high growth temperatures in combination with high flow rates of the dopant precursor silane in order to obtain highly Si-doped $Al_{0.72}Ga_{0.28}N$ layers can reduce the concentration of carriers which correlates with the reduced amount of silicon incorporated as a donor into the layers. The formation of coverage of Si-N bonds at the higher process temperatures used in combination with a high $SiH_4$ flow rate is speculated as a conceivable mechanism, which can possibly operate in combination with other outlined effects.

## Acknowledgements

Partial support from the Linköping Linnaeus Initiative for Novel Functional Materials (LiLi-NFM, VR) is acknowledged. A.K.G. acknowledges support from the Swedish Governmental Agency for Innovation Systems (VINNOVA) and Swedish Research Council (VR). We thank Dr M. Kappers for discussion and critical reading of the manuscript.

## Notes and references

1 D. D. Koleske, A. E. Wickenden, R. L. Henry and M. E. Twigg, *J. Cryst. Growth*, 2002, **242**, 55.
2 Y. Mols, M. R. Leys, E. Simons, J. Poortmans and G. Borghs, *J. Cryst. Growth*, 2007, **298**, 758.
3 A. Kakanakova-Georgieva, U. Forsberg, I.G. Ivanov, E. Janzén, *J. Cryst. Growth*, 2007, **300**, 100.
4 J.-T. Chen, U. Forsberg and E. Janzén, *Appl. Phys. Lett.*, 2013, **102**, 193506.
5 T. F. Kuech, R. Potemski, F. Cardone and G. Scilla, *J. Electr. Mater.*, 1992, **21**, 341.
6 S. Keller, P. Cantu, C. Moe, Y. Wu, S. Keller, U.K. Mishra, J.S. Speck and S.P. DenBaars, *Jpn. J. Appl. Phys.*, 2005, **44**, 7227.
7 A. Kakanakova-Georgieva, D. Nilsson, X. T. Trinh, U. Forsberg, N. T. Son and E. Janzén, *Appl. Phys. Lett.*, 2013, **103**, 132113.
8 A. Kakanakova-Georgieva, D. Nilsson, X.T. Trinh, N.T. Son and E. Janzén, *Solid State Phenomena*, 2014, **205-206**, 441.
9 T. Mattila and R.M. Nieminen, *Phys. Rev. B*, 1996, **54**, 16676.
10 L. Silvestri, K. Dunn, S. Prawer and F. Ladouceur, *Appl. Phys. Lett.*, 2011, **99**, 122109.
11 D.J. Chadi and K.J. Chang, *Phys. Rev. Lett.*, 1988, **61**, 873.
12 L. Gordon, J. L. Lyons, A. Janotti and C. G. Van De Walle, *Phys. Rev. B*, 2014, **89**, 085204.
13 D.V. Lang and R.A. Logan, *Phys. Rev. Lett.*, 1977, **39**, 635.
14 M.D. McCluskey, N.M. Johnson, C.G. Van de Walle, D.P. Bour, M. Kneissl and W. Walukiewicz, *Phys. Rev. Lett.*, 1998, **80**, 4008.
15 R. Zeisel, M.W. Bayerl, S.T.B. Goennenwein, R. Dimitrov, O. Ambacher, M.S. Brandt and M. Stutzmann, *Phys. Rev. B*, 2000, **61**, R16283.
16 P.M. Mooney, W. Wilkening, U. Kaufmann and T.F. Kuech, *Phys. Rev. B*, 1989, **39**, 5554.
17 X.T. Trinh, D. Nilsson, I.G. Ivanov, E. Janzén, A. Kakanakova-Georgieva and N.T. Son, *Appl. Phys. Lett.*, 2014, **105**, 162106.
18 N.T. Son, M. Bickermann and E. Janzén, *Appl. Phys. Lett.*, 2011, **98**, 092104.
19 M. L. Nakarmi, K. H. Kim, K. Zhu, J. Y. Lin and H. X. Jiang, *Appl. Phys. Lett.*, 2004, **85**, 3769.
20 R. Collazo, S. Mita, J. Xie, A. Rice, J. Tweedie, R. Dalmau and Z. Sitar, *Phys. Status Solidi C*, 2011, **8**, 2031.
21 F. Mehnke, T. Wernicke, H. Pingel, C. Kuhn, C. Reich, V. Kueller, A. Knauer, M. Lapeyrade, M. Weyers and M. Kneissl, *Appl. Phys. Lett.*, 2013, **103**, 212109.
22 Evans Analytical Group® (EAG), http://www.eaglabs.com
23 D. Nilsson, X.T. Trinh, E. Janzén, N.T. Son and A. Kakanakova-Georgieva, *Phys. Status Solidi B*, 2015, **252**, 1306.
24 S. Tanaka, M. Takeuchi and Y. Aoyagi, *Jpn. J. Appl. Phys.*, 2000, **39**, L831; S. Tanaka, S. Iwai, and Y. Aoyagi, Appl. Phys. Lett., 1996, **69**, 4096.
25 M. Kasu and N. Kobayashi, *Appl. Phys. Lett.*, 2001, **78**, 1835.
26 T. Markurt, L. Lymperakis, J. Neugebauer, P. Drechsel, P. Stauss, T. Schulz, T. Remmele, V. Grillo, E. Rotunno and M. Albrecht, *Phys. Rev. Lett.*, 2013, **110**, 036103.
27 N. Kuwano, M. Hijikuro, S.Hata, M. Takeuchi, and Y. Aoyagi, J. Cryst. Growth, 2007, **298**, 284.
28 S.-L. Sahonta, M. Q. Baines and D. Cherns, *Phys. Status Solidi B*, 2002, **234**, 952.
29 A. E. Romanov and J. S. Speck, *Appl. Phys. Lett.*, 2003, **83**, 2569.
30 D. M. Follstaedt, S. R. Lee, A. A. Allerman and J. A. Floro, *J. Appl. Phys.*, 2009, **105**, 083507.
31 A. E. Romanov, G. E. Beltz P. Cantu, F. Wu, S. Keller, S. P. DenBaars, and J. S. Speck, *Appl. Phys. Lett.*, 2006, **89**, 161922.
32 I. C. Manning, X. Weng, J. D. Acord, M. A. Fanton, D.W. Snyder, and J.M. Redwing, *J. Appl. Phys.*, 2009, **106**, 023506.
33 S. Kurai, F. Ushijima, H. Miyake, K. Hiramatsu, and Y. Yamada, J. Appl. Phys., 2014, **115**, 053509.
34 S.F. Chichibu, H. Miyake, Y. Ishikawa, M. Tashiro, T. Ohtomo, K. Furusawa, K. Hazu, K. Hiramatsu and A. Uedono, *J. Appl. Phys.*, 2013, **113**, 213506.
35 C. G. Van de Walle, and J. Neugebauer, *Mat. Res. Soc. Symp. Proc.*, 1996, **395**, 645.
36 A.M. Armstrong, M.W. Moseley, A.A. Allerman, M.H. Crawford, and J.J. Wierer, Jr., *J. Appl. Phys.*, 2015, **117**, 185704.